REGIONAL VARIABILITY IN TROPICAL CONVECTION: OBSERVATIONS FROM TRMM

By

Walter A. Petersen[*] and Steven A. Rutledge

Department of Atmospheric Science
Colorado State University
Fort Collins, Colorado 80523-1371

[*] *Corresponding author*: Dr. Walter A. Petersen, Department of Atmospheric Science, Colorado State University, Fort Collins, CO. 80523-1371. e-mail: walt@radarmet.atmos.colostate.edu

Abstract

Observation of the vertical profile of precipitation over the global tropics is a key objective of the Tropical Rainfall Measuring Mission (TRMM) because this information is central to obtaining vertical profiles of latent heating. The present study combines both TRMM Precipitation Radar (PR) and Lightning Imaging Sensor (LIS) data to examine *"wet-season"* vertical structures of tropical precipitation across a broad spectrum of locations in the global tropics. TRMM-PR reflectivity data (2A-25 algorithm) were utilized to produce seasonal mean three dimensional relative frequency histograms and precipitation ice-water contents over grid boxes of approximately 5°-10° in latitude and longitude. The reflectivity histograms and ice water contents were then combined with LIS lightning flash densities and 2A-25 mean rainfall rates to examine regional relationships between precipitation vertical structure, precipitation processes, and lightning production.

Analysis of the reflectivity vertical structure histograms, and lightning flash density data reveal that 1) relative to tropical continental locations, wet-season isolated tropical oceanic locations exhibit relatively little spatial (and in some instances seasonal) variability in vertical structure across the global tropics; 2) coastal locations and areas located within 500-1000 km of a continent exhibit considerable seasonal and spatial variability in mean vertical structure, often resembling "continental" profiles or falling intermediate to that of tropical continental and isolated oceanic regimes; and 3) interior tropical continental locations exhibit marked variability in vertical structure both spatially and seasonally, exhibiting a continuum of characteristics ranging from a near isolated oceanic profile observed over the central Amazon and India, to a more robust continental profile observed over regions such as the Congo and Florida. Examination of regional and seasonal mean conditional instability for a small, but representative subset of the geographic locations suggests that tropospheric thermodynamic structure likely plays a significant role in the regional characteristics of precipitation vertical structure and associated lightning flash density.

In general, the largest systematic variability in precipitation vertical structure observed between all of the locations examined occurred above the freezing level. *Importantly, sub-freezing temperature variability in the vertical reflectivity structures was well reflected in the seasonal mean lightning flash densities and ice water contents diagnosed for each location. In turn, systematically larger rainfall rates were observed on a pixel-by-pixel basis in locations with larger precipitation ice water content and lightning flash density. These results delineate, in a regional sense, the relative importance of mixed phase precipitation production across the global tropics.*

1. Introduction

In addition to accurately quantifying the horizontal distribution of rainfall in the global tropics, the observation of corresponding vertical profiles of precipitation in deep tropical convection is also a key objective of the Tropical Rainfall Measuring Mission (TRMM; Simpson et al., 1988). While the horizontal distributions of rainfall yield important information on both the magnitude and location of column-integrated net latent heat release in the troposphere, vertical profiles of precipitation and hydrometeors can yield specific information on where the latent heating is taking place in the vertical (e.g., Tao et al., 1990,1993; Yang and Smith, 1999; Olson et al., 1999). Note that the latent heat release in deep convection comprises a large fraction of the total diabatic heating budget (e.g. Riehl and Malkus, 1958; Tao et al, 1990). More importantly, the *vertical gradient* of this localized heating is manifested as divergence (e.g., Mapes and Houze, 1993), resulting in a thermally forced dynamical response in the tropical atmosphere to convection that has been both observed and modeled over a broad spectrum of temporal and spatial scales (Hartman et al., 1984; DeMaria, 1985, Lau and Peng, 1987; Sui and Lau, 1989; Mapes, 1993; Mapes and Houze, 1993; Puri, 1994). In turn, the dynamical responses to the heating can feedback to the entire atmospheric general circulation through a variety of regional and global teleconnections (Horel and Wallace, 1981; Hartman et al., 1984; Trenberth et al., 1988). For these reasons, one of the primary goals of TRMM is to characterize the four-dimensional (4-D) structure of latent heating in the tropics.

Obtaining a *direct* measurement of the latent heat release occurring in convection over the entire tropics is not possible. However, remote sensing of cloudiness and precipitation structure over the tropics in both the horizontal and vertical planes, though non-trivial, is possible utilizing instrument platforms such as the TRMM satellite. The TRMM satellite is in a 35° inclination non-sun synchronous low-earth orbit (launched in late November 1997), and carries a suite of five instruments (Kummerow et al., 1998). The instrument package includes the 13.8 GHz TRMM Precipitation Radar (PR), the multi-frequency TRMM Microwave Imager (TMI), a multi-frequency Visible and Infrared Radiometer (VIRS), the

Lightning Imaging Sensor (LIS; Christian et al., 1999), and the Clouds and Earth Radiant Energy System (CERES). The PR, TMI and VIRS are explicitly identified in the TRMM science plan (cf. Kummerow et al., 1998) as the *primary* rainfall measurement instruments. Once collected and quality controlled, the precipitation measurements are utilized in an inversion process relying on sophisticated cloud and radiative transfer models that utilize both rainfall and convective structure observations to provide estimates of the magnitude and vertical profile of latent heating in the tropics (e.g., Tao et al., 1990,1993; Kummerow and Giglio, 1994a,b; Olson et al., 1999). Heretofore the list of "primary" precipitation measurements and the rainfall/heating algorithms have not directly involved LIS lightning observations. One goal of the present study is to demonstrate the complementary use of such observations for the diagnosis of regional variability in both convective vertical structure and precipitation processes.

On one hand, the exclusion of lightning observations in the TRMM algorithms is surprising as decades of lightning research have demonstrated correlations between the presence or absence of lightning and numerous TRMM-relevant cloud characteristics including the presence or absence of mixed-phase microphysics, hydrometeor types, updraft strength, and convective rainfall (cf. MacGorman and Rust, 1999 for a review). The fundamental relationship between ice microphysics and electrification (cf. MacGorman and Rust, 1999) suggests that at least *some* basic relationships should exist between lightning frequency, cloud structural characteristics and rainfall. However, the development of *robust quantitative* relationships, for example, relating lightning flash rates to cloud microphysical and kinematic features, has proven to be difficult. This is especially true for applications in synoptic to global scale diagnostic studies of convection. However, with the recent advent of accurate global and continental-scale lightning detection (e.g., Lee et al. 1986; Cummins et al., 1998; Chang et al., 1999; Christian et al., 1999) the application of lightning data to a wide variety of synoptic and climate scale meteorological problems is now quite feasible (e.g., assimilation of lightning data into numerical models to improve forecasts, Alexander et al., 1999, Chang et al., 1999; ENSO applications reported in Goodman et al., 2000; refinements in space-borne precipitation estimation, Grecu et al., 2000; correlations between global lighting flash rate variability and upper tropospheric water vapor; Price, 2000).

It is well established that periodic spatial/temporal global and regional scale variations in atmospheric forcing (thermodynamic/dynamic) modulate the occurrence and intensity of deep convection. In turn, 4-D variability in deep convection is well reflected in observations of the temporal and spatial variability of lightning (Rutledge et al., 1992; Jayaratne, 1993; Williams and Renno 1993; Goodman and Christian, 1993; Williams 1992,1994; Kent et al., 1995; Petersen et al., 1996; Fullekrug and Frazer-Smith, 1997; Hidayat and Ishii, 1998; Satori and Zeiger, 1998, 1999; Manohar et al., 1999; Reeve and Tuomi, 1999; McCollum et al., 2000; Anyamba et al., 2000; Goodman et al., 2000; Nesbitt et al., 2000; Boccippio et al., 2000; Torracinta and Zipser, 2000). The physical basis for these correlations is rooted in the synergistic relationship between cumulonimbus cloud kinematics, microphysics and electrification. For example, when/where larger or more numerous cumulonimbi possessing relatively strong updrafts occur (e.g., ≥ 6 m s^{-1} near the freezing level of oceanic convection; Zipser and Lutz, 1994; Petersen et al., 1999), resultant enhancements in mixed phase cloud microphysics are expected, more electrical charge is generated (e.g., Takahashi, 1978; Saunders et al., 1991), and subsequently more lightning is produced. Indeed, relationships between kinematics, microphysics and lightning have certainly been observed for individual cloud systems. Hence we might expect to find similar, or even stronger, correlations (due to the averaging process) between parameters rooted in the kinematics and microphysics of cumulus *cloud ensembles* and lightning, when both are observed over relatively large spatial (e.g., 5°x5° boxes) and/or long temporal (e.g., monthly or longer) scales.

For example, on temporal and spatial scales similar to that of the highest level products derived from TRMM (monthly, 5°x5° grid boxes), Petersen and Rutledge (1998) found systematic changes in the ratio between rainfall and cloud-to-ground lightning (termed the rain yield) which were argued to be the result of identifiable shifts in the convective regime. Large ratios (10^9-10^{10} kg/flash) were noted for monsoon/oceanic rainfall regimes, while smaller ratios (10^7-10^8 kg/fl) were noted for continental regimes. Williams et al. (1992) and Hidyat and Ishii (1998) found similar shifts in the rain yield when examining monsoon and continental rainfall regimes near Darwin, Australia (Java). Zipser (1994) and Manohar (1999) noted similar transitions in the ratio of rainfall to thunderdays when examining the occurrence of

thunderstorms and rainfall occurring in monsoon, oceanic and continental regimes. Petersen and Rutledge (1998) suggested that the correlation between the rainfall and lightning should be strongest where ice-phase microphysics (as opposed to warm-rain processes) play a dominant, but not necessarily exclusive role in the production of rainfall, consistent with the correlation between rainfall and lightning being strongest over interior continental regions in their study.

More recently, Nesbitt et al. (2000) utilized a three month global tropical sample of TRMM PR, LIS and TMI data and found that for equal area normalized rainfall over land and ocean, lightning flash rates were much lower over the ocean (consistent with lower 30 dBZ reflectivity heights), suggesting a decoupling of the microphysics responsible for rainfall production (e.g., strong warm-rain component) relative to that necessary for lightning production (robust mixed phase) in oceanic convection. In a related study utilizing TRMM-TMI measurements, Torracinta and Zipser (2000) found that a small percentage of the tropical oceanic convection in their sample exhibited 85GHz ice scattering signatures similar to that of continental convection. However, this small percentage of oceanic convection was still less likely to produce lightning relative to convection associated with similar brightness temperatures observed over continents, suggesting perhaps the presence of different ice microphysical processes in the two types of convection.

Studies such as Rutledge et al. (1992), Williams et al (1992), Zipser (1994), Petersen and Rutledge (1998), Nesbitt et al. (2000), and Torracinta and Zipser (2000) are good examples (amongst many) of studies that have utilized different types of remote sensing including raingauge, radar, lightning, and passive microwave observations to infer qualitative differences in the mean vertical structure of precipitation and associated microphysical processes between regime dependent types of convection (e.g., oceanic, monsoon, and land). This variability between regimes, with corresponding differences in convective structure and microphysical processes, are clearly important to the overarching goals of TRMM.

Given approximately three years of global tropical coverage afforded by the TRMM satellite (and a projection of 4 more years; personal communication, Prof. C. Kummerow), and the dependence of

regional latent heat retrievals on accurate cumulus ensemble modeling of cloud microphysical and kinematic properties (e.g., Tao et al., 1993; Olson et al., 1999), it is now important to pursue the identification of regional or regime driven variations in convective vertical structure and their associated effects on rainfall and cloud microphysical processes. In this study we use TRMM PR and LIS data collected over a time period from December 1997 to February 2000, to conduct statistical studies of the vertical structure of convection over a wide variety of locations in the global tropics. By combining analyses of TRMM LIS and PR reflectivity statistics over these locations, conclusions are drawn regarding variability in the microphysical and kinematic structures of the convective ensembles observed. We also explore the quantitative relationship between lightning flash density and other cloud ensemble "outputs" such as precipitation and ice-water content. Given the relationship between latent heating and the microphysical/kinematic structure of convection, *another goal of this study is to take one more step toward the creation of a unified framework from which to describe the variability of the vertical structure of tropical convection as it relates to its kinematic, microphysical, electrical, and latent heating characteristics.*

2. Methodology

In order to sample a representative cross-section of convective vertical structures and accompanying lightning flash counts in a diverse set of tropical locations and to describe those data over spatial and temporal scales consistent with TRMM objectives (5°-10° x 5°-10° boxes, monthly timescales), approximately 22 rectangular areas of dimension O[5°x5°] were selected for study (Table 1; Figs. 1a-b). The selection of a specific analysis rectangle was determined by either its geographical location relative to TRMM interests (e.g., whether a rectangle was located over a ground validation or field campaign site etc.), and/or by observed seasonal patterns in heavy rainfall and lightning. The areas thus selected are distributed over all the continental landmasses and ocean basins found in the tropics (e.g., Table 1).

Two primary datasets served as the basis for analysis: 1) TRMM-PR 2A-25 algorithm volumetric radar reflectivities and rainfall rates (Iguchi and Meneghini, 1994; Kummerow et al., 1998; Meneghini et

al., 1999); and 2) TRMM-LIS lightning "flash" locations (Christian et al., 1999; Boccippio et al., 2000). Raw TRMM-LIS lightning flash data were first gridded by computing monthly total lightning flash densities (flashes/km^2/mo) for 0.5° x 0.5° grid boxes over the entire tropics. This "processed" lightning data set was then used for examining both spatial and temporal variations of lightning[1] and for computing seasonal (e.g., 3 months) mean lightning flash densities in each of the 20 rectangular boxes.

The TRMM-PR data were composited to produce three-dimensional *seasonal* mean relative frequency histograms of reflectivity (Z) by tabulating pixels (4.3 km footprint; Kummerow et al., 1998) located in each analysis rectangle over 5 dBZ reflectivity bins, and 1 km height bins (four gates per height bin) in the elevation range from 2 km to 18 km. Only rays containing reflectivity pixels classified as "rain-certain" by the 2A-25 algorithm and possessing reflectivity ≥ 20 dBZ (near the TRMM-PR noise threshold) were included in the histograms. In essence the 3-D histograms represent the conditional probability of finding reflectivities in a given 5-dBZ reflectivity bin of a precipitating cloud population at a certain height level (cf., Yuter and Houze, 1995; DeMott and Rutledge, 1998a). In order to highlight "intense" convection, especially at altitudes above the freezing level, similar histograms were also constructed for reflectivities in excess of 30 dBZ. No convective-stratiform partitioning (e.g., Steiner et al., 1995) of the echo contained in the histograms was attempted in this study, nor was this required for our objectives.

During construction of the histograms, individual reflectivity pixels were also converted to precipitation Ice Water Contents (IWC's; g m^{-3}) for each 1 km height bin above the 7 km level (-12° to –15°C) utilizing an exponential size distribution and resultant reflectivity-IWC (Z-M) relationship:

$$ \text{IWC} = 1000\pi\, \rho_i\, N_0^{3/7} \left(\frac{5.28 \times 10^{-18}}{720} Z \right)^{4/7} \qquad \text{g m}^{-3} \qquad (1) $$

where N_0 = 4 x 10^6 m^{-4}, and ρ_i = 917 kg m^{-3}.

---

[1] The lightning data include both intracloud and cloud-to-ground components.

This particular IWC-Z relationship for tropical convection was presented in Carey and Rutledge (2000). Note that the N_0 selected for this relationship is not particularly unique, but was chosen based on comparisons between cloud modeling simulations and observations of both tropical island and oceanic convection (Petersen, 1997). The 7 km height level was selected in order to provide some assurance that the reflectivities would, in the mean, be dominated by precipitation-sized ice particles as opposed to raindrops. Individual IWC's were then averaged in each height bin to create layer mean IWC's. The quantitative validity of the IWC's utilizing only a single Z-M relationship for the whole tropics is somewhat dubious (which could be inferred from the results of Torracinta and Zipser, 2000), as many other Z-M relationships exist in the literature and reflect variations in both regime and cloud-system type (cf., Black, 1990). However, the spatial and temporal *trends* in the IWC, as opposed to the computed values are what will be emphasized in this study.

In addition to computing IWC's above the 7 km height level, the percentage of reflectivity pixels in a grid column exceeding 30, 35, 40 and 45 dBZ located above the 7 km height level (herein defined as "intense" convection based on a high probability of lightning; e.g., Dye et al., 1989; Zipser and Lutz, 1994; Petersen et al., 1996; Nesbitt et al., 2000) was also computed. This percentage was computed utilizing a denominator assigned to be either the total number of raining pixels observed above the 2 km level (e.g., percentage of the total observed population), or the total number of raining pixels observed above the 7 km level (e.g., a percentage of the "deep" convection). In this fashion regional percentages, or conditional probabilities, of: a) intense convective pixels occurring in raining portions of a given rectangular area; and b) intense convection occurring in the subset of pixels associated with "deep" convective towers, could be evaluated and later compared to regional lightning flash densities and mean layer IWC's.

Lastly, rainfall rates computed for each pixel in the 2A25 algorithm were averaged in the 2-3 km height layer over each region for comparison to lightning flash data, precipitation IWC, and the fraction of pixels exceeding 30 dBZ located above the 7 km level. This was undertaken to evaluate in relative

terms the contribution of precipitation ice processes in deep convection to mean rainfall rates in each region.

3.   Regional variability revealed in lightning characteristics

We begin discussion by considering the distribution of mean lightning flash density detected by the TRMM-LIS for the austral (Dec.-Feb.) and boreal (Jun-Aug) summer seasons of 1998-2000 (Figs. 1a-b). Several features in both the distribution of lightning flashes and convective vertical structure can be inferred from Figs. 1a-b. First, and as shown in numerous previous studies (Kotaki and Kato, 1983; Orville and Henderson, 1986; Christian et al., 1999), it is clear that global tropical lightning flash densities are dominated by convection occurring over land masses. Over isolated oceanic regions (e.g., not likely to be influenced by a nearby landmass), lightning tends to occur in recognized convergence zones such as the ITCZ, South Pacific Convergence Zone (SPCZ), and South Atlantic Convergence Zone (SACZ), but with flash densities roughly 10-100 times smaller than that of tropical land masses. Finally, there are preferred regions of lightning occurrence located in coastal margins or within 500-1000 km of major land masses, some of which exhibit flash densities comparable to that observed over land (e.g., the warm waters of the Gulf Stream located off the east coast of the U.S.).

If maps of lightning (Figs. 1a), rainfall (Fig. 2a), and Outgoing Longwave Radiation (OLR; Fig. 2b) are compared, regional differences in convective structure become readily apparent. In the most obvious case, differences in convective structure can be readily inferred if one compares lightning, rainfall and OLR over land and ocean regimes. However, this is also true when comparing continental areas, and coastal oceanic to isolated oceanic regimes. For example, consider the austral summer mean rainfall and OLR observed in the tropical rainforest regions of the Amazon (60° W, 10° S) and the Congo (23° E, 10°S) shown in Figs. 2a-b. Both of these regions are associated with significant rainfall ($\geq$ 5 mm day^{-1}; Fig. 2a), with the Amazon exhibiting heavier rainfall than the Congo. Note that OLR values (Fig. 2b) vary in a consistent fashion with the aforementioned differences in rainfall, suggesting perhaps that convection over the Amazon (AMZ) is either deeper, more frequent and/or more intense than that of the

Congo. However, based on lightning flash densities (Fig. 1a), the Congo appears to be the location of more intense, or at least more vertically developed convection. Indeed passive microwave observations presented in Mohr et al. (1999) suggest that convection over the Congo is more vertically developed than that of the Amazon consistent with the lightning observations, but area coverage of mesoscale convective systems is larger in the AMZ (Mohr et al., 1999) consistent perhaps with the presence of more rainfall and reduced OLR's in the AMZ. Even more local to the AMZ (e.g., on the same continent), note that similar regional differences in convective structure likely exist when the AMZ and regions of sub-tropical south-central Brazil (e.g., the Mato Grosso) are compared.

While we have considered spatial variability in regional lightning activity and inferred convective structure, there also temporal variations to consider. Consider again a comparison of lightning activity between the AMZ and the Congo during the austral spring (transition to wet season; Fig. 3). Seasonally, the transition to the wet season in the AMZ is still associated with copious rainfall (≥ 4 mm day^{-1} via the CMAP rainfall product; Xie and Arkin, 1997) but the lightning activity is markedly increased (Fig. 3) and quite similar to that observed in the Congo, the Maritime Continent region, and in other regions of sub-tropical South America.

It is interesting to note that the recent TRMM-LBA field campaign (Rutledge et al., 2000) was conceived with the goal of sampling convection "typical" of an "interior" continental regime during the wet season (TRMM Science Operations Plan, Executive Summary; 1996). However, based on the lightning, rainfall and OLR data the vertical structure of wet season convection in the AMZ must be different from that of the Congo or even that of the Maritime Continent region (cf. Figs.1-2). During the transition season of Sep.-Nov.. the same data suggest that convection in the AMZ may take on characteristics that are more similar to the Congo and Maritime Continent region- perhaps this is the sought after "typical interior" continental convective regime. What does the vertical structure of this convection look like and how does it compare to other locations in the global tropics? We address this question in the following section.

4. PR-Diagnosed convective vertical structure

Three-dimensional TRMM-PR Relative Frequency Distributions for Reflectivities (RFDR's) are shown in Figs. 4-6 for representative tropical oceanic and continental rainfall analysis boxes (e.g., Table 1; Figs. 1a-b, 3). The RFDR's are truncated at an elevation of 15 km (~ tropopause height) to eliminate the effects of noise (e.g., side lobe clutter) on the distribution due to the relatively small number of points (≤ 1% of the total) present in the sampling distribution above that level. Each RFDR represents mean *wet-season* precipitation vertical structure for a given analysis box. By focusing on wet-seasons, relative comparisons between different locations for seasons of peak latent heat release can be made. In a relative sense, variability in the RFDR's between comparable periods of peak latent heat release should also indicate variability in the mean latent heating profiles (e.g., Tao et al., 1990, 1993; DeMott and Rutledge, 1998b; Cartwright and Ray, 1999).

From the perspective of wet-season variability, PR RFDR's computed for Isolated-Oceanic regimes (IO) exhibit the least amount of variation between individual analysis regions (Figs. 4a-d). To first order, the IO RFDR's exhibit significant precipitation mass (e.g., $Z \geq 30$ dBZ) confined to elevations below the freezing level (~5km). Both the reflectivity structure and the overall similarity between reflectivity structures are maintained for the isolated oceanic regimes even when considering other seasons (not shown). Previous observations of oceanic convection over both the Pacific and Atlantic basins (e.g., Szoke et al., 1986; Jorgensen and LeMone, 1989; Zipser and Lutz, 1994; Takahashi et al., 1995; Petersen et al., 1996, 1999; DeMott and Rutledge, 1998a) suggest the presence of deep cloud systems, efficient warm-rain processes and heavy convective rainfall, but relatively weak vertical motion and structure (consistent with overall weaker mixed-phase ice processes and relative decreases in lightning flash density; Fig. 1). These features are universally evident in Figs. 4a-d for convection sampled by the TRMM-PR over *all* of the ocean basins, and are characterized by the near absence (dominance) of reflectivities ≥ 30 dBZ above (below) the freezing level (~5 km) and a near constant (relative frequency = 0.8-0.9) dominance of reflectivities ≤ 25 dBZ above the freezing level extending to tropopause heights (e.g., a deep column of smaller ice particles). In terms of intensity, if the height of 30 dBZ echoes is

considered as a metric of "intensity" (e.g., Petersen et al., 1996; DeMott and Rutledge, 1998a,b) then Fig. 4 indicates that convection over the western Pacific warm-pool is slightly more intense than that sampled over the other ocean regions. This slight increase in convective intensity found in the western Pacific warm-pool RFDR is somewhat suggested by the lightning flash data (Figs. 1a-b) and may be linked to the location of the warm-pool analysis box relative to the location of the SPCZ (e.g., compare Fig. 4a to Fig. 4d located in the northern hemisphere portion of the warm-pool).

Based on numerous previous studies and the aforementioned IO RFDR's discussed in this study, it might be tempting to conclude that a consensus has been reached regarding the basic structure and intensity of *all* tropical oceanic convection. However, caution must be taken when assigning the classification of "tropical oceanic convection". The RFDR's shown in Figs. 4a-d are for *isolated* regions of ocean (i.e., those locations located a distance >1000 km from any coastline). If regional RFDR's are considered for oceanic regimes located within 1000 km of a coastline (identified herein as "coastal"), the structural characteristics of the convection relative to the isolated oceanic regimes change markedly, though not necessarily in a uniform fashion (e.g., Figs. 5a-d).

For example, coastal convection occurring over the Gulf Stream (southeast of the U.S. States of South and North Carolina) during boreal summer exhibits a more robust vertical structure than any of the aforementioned IO areas shown in Figs. 4a-d. The increased convective intensity is further manifested in Fig. 1b by considering the increased flash densities observed in the Gulf Stream analysis box (29°-34° N, 77°-72° W) relative to neighboring continental and oceanic areas. Relative to IO regimes, slight increases in convective intensity are also present over the South China Sea (Fig. 5b), Gulf of Mexico (Fig. 5c), and to a lesser extent over the Mexican warm-pool in the eastern Pacific Ocean (Fig 5d). It is important to note however, that the "coastal" regimes do not exhibit the first order similarity in convective vertical structure observed to occur between the different IO RFDR's. That is, regional variability in the convective structure and intensity of coastal-influenced convection during wet-seasons is the rule. This variability was also observed in a temporal sense when different seasonal RFDR's were compared for the same and/or different analysis locations (not shown).

In contrast to both the similarity and weaker intensity of the IO RFDR's, the continental RFDR's exhibit markedly different characteristics (Figs. 6a-d), similar to the behavior noted for the coastal regimes. First, the shapes of the continental RFDR's vary substantially by location, especially if reflectivities ≥ 25 dBZ are considered. Second, relative to the IO profiles (and consistent with the lightning data) the continental convection is generally more intense, though, to a varying degree. Note that all of the continental profiles in Figs. 6a-d suggest a larger relative percentage of reflectivities ≥ 30 dBZ at levels above 5 km, consistent with an overall preference for lightning to occur over land (Figs. 1a-b). One other characteristic of the "continental" RFDR's is the peakedness in frequency of the 20-25 dBZ bin between the 5 km and 10 km levels. Comparing Figs. 4-6 it is clear that the more "continental" a reflectivity distribution becomes, the more pronounced the peakedness in RFDR 20-25 dBZ values becomes above the 5 km level. Conversely, the distribution of 20-25 dBZ reflectivities over isolated ocean tends to be flat above the 5 km level, while the coastal RFDR's exhibit a mixture of continental and oceanic shapes depending on location. The exact cause of the peakedness in the 20-25 dBZ frequencies above 5 km over the continents is not clear, however recent observations collected during TRMM-LBA (and elsewhere; e.g., Rutledge and Petersen, 1994) suggest that this signal may be related to the presence of more vertically developed MCS stratiform region precipitation located over the continents (responsible for the 20-25 dBZ peak in the 5-10 km layer) coupled with a more frequent deep convective mode that produces a larger percentage of storms associated with robust precipitation ice phase above the 7 km level (hence larger echo intensities and more lightning). Essentially, the 20-25 dBZ peakedness trend suggests that the precipitation echo-top populations over the continents (or continental-like regimes) exhibit a different modal structure compared to that of IO regions (e.g., Johnson et al., 1998).

The structural differences observed between continental and IO RFDR's may be a strong reflection of the ever-increasing role that ice processes play in rainfall production over the continents. However, it is clear from Figs. 4-6 that the relative contribution of various microphysical processes to precipitation production cannot be clearly assessed using only a simple partitioning scheme based on "continental" or "oceanic" geographical identifiers, since even convection that is technically occurring over the ocean can

look continental (e.g., Fig. 5a), and vice versa (e.g. Figs. 6a and 6c). This is evident in the RFDR's shown in Fig. 7 for nine locations (including seasonal variations for two locations) that were selected as being broadly representative of the 22 total locations examined (Table 1).

The color scheme in Fig. 7 indicates the relative grouping of a given location based primarily on geography (e.g., land, ocean or coastal), with the exception of the continental Amazon *wet-season* data point (and pronounced monsoon locations such as southern India; Table 1) which, for the purpose of further discussion, was indicated as a separate group. In general, the RFDR's shown in Fig. 7 exhibit a marked continuous trend in regional precipitation structure suggesting a tendency for the most vertically developed convection (based on frequency of 30 dBZ above the 7 km level) to occur over sub-tropical locations (continental and coastal), followed by continental Tropical locations and finally isolated regions of tropical ocean. Below the 5 km level, reflectivity structures observed in the various regimes are somewhat similar, with only a slight tendency for the continental and Gulf Stream coastal regimes to exhibit higher frequencies of reflectivity in excess of 30 dBZ (~10%). For heights exceeding 5 km, Fig. 7 suggests a more pronounced difference in the RFDR's. Given that a 20 dBZ reflectivity is observed in pixels above heights of ~6 km, the range of relative frequencies $\geq$ 30 dBZ from land to oceanic convection spans a maximum difference of 23%, a factor of two larger than that observed below the 5 km level. *Hence the largest systematic variability observed between regional wet-season vertical precipitation structures is found above the freezing level. The variability at sub-freezing temperatures is reasonably reflected in the distributions of lightning flash density shown in Figs. 1a-b (cf. Sec. 5).*

As a more specific example, consider the AMZ and Congo region RFDR's (Figs. 6a, 6c, and 7) relative to their respective lightning (Figs. 1a, and 3), rainfall (Fig. 2a) and OLR characteristics (Fig. 2b). The AMZ and Congo analysis boxes are both at approximately the same latitude, covered by dense tropical rainforest, and bordered by mountains on one side and ocean on the other (distant). Both regions can certainly be considered "interior" to a tropical continent. Comparing the $\geq$ 30 dBZ RFDR's between the AMZ and the Congo and other locations in Fig. 7, the vertical structure of heavy precipitation over the AMZ during the transition season (Sept.-Nov.; ~2/3 of the wet-season rainfall) strongly resembles that of

13

the Congo and other tropical continental locations (e.g., Fig. 7). However, during the December-February *wet-season*, the AMZ reflectivity structure exhibits characteristics that more closely resemble those of the IO (Figs. 4a-d) and South China Sea locations (Fig. 5b). As suggested by the groupings in Table 1, similar behavior is also observed in the reflectivity statistics for S. India when the monsoonal period of June-August (Fig. 6d) and the Sept.-Nov. post-monsoon timeframe are compared (Fig. 7). Interestingly, no similar variability was observed seasonally in RFDR or LIS data for the Congo (accounting for north-south seasonal migrations of the convection).

The observed AMZ *wet-season* TRMM-PR precipitation structure is consistent with passive microwave observations (85 GHz) summarized in Mohr et al. (1999) who reported wet-season ice scattering characteristics over the AMZ similar to those observed over the tropical oceans. However, the AMZ *transition-season* statistics (Fig. 7) combined with the LIS data (Fig. 3) indicate a marked seasonal variability in the RFDR suggesting that the wet-season results summarized in Mohr et al. (1999) for the AMZ do not apply year round. Mohr et al. (1999) noted that convection in the Congo exhibited the coldest 85 GHz brightness temperatures observed in the tropics, by proxy, an indicator of greater convective intensity and more robust precipitation ice processes. When considered with the observed relative seasonal invariance of the TRMM-PR RFDR over the Congo, it seems likely that the passive microwave statistics summarized in Mohr et al. (1999) for the Congo *may be representative* of the convection occurring therein, regardless of the season.

Combined with the OLR, rainrate and lightning observations, the difference in vertical structure observed between the AMZ, Congo and other continental locations and indeed, between locations dominated by a summer monsoon such as India (Figs. 6d; 7), suggest that marked regional differences exit in the cloud microphysical (e.g., McCollum et al., 2000) and kinematic processes of several regimes. What atmospheric parameters contribute to these differences in structure?

Recent studies have offered plausible explanations involving aerosol loading to explain differences in both the precipitation structural and electrical characteristics observed between *geographically similar* locations in the tropics (e.g., Rosenfeld and Lentsky, 1998; Williams et al., 2000; McCollum et al., 2000).

However, it also seems intuitive to consider parameters related to the column-integrated instability (e.g., Convective Available Potential Energy; CAPE) and/or the vertical profile of thermodynamic instability, which fundamentally exert strong controls over both the intensity and frequency of convection. To the extent that thermodynamic controls represent a first order effect on regional mean convective structure, we expect to see regional differences in tropospheric thermodynamic structure (e.g., in conditional instability; CI) that are consistent with the observed differences in regional mean convective structure (e.g., Figs. 4-7) and lightning flash density (e.g., Figs. 1 and 3; Williams and Renno, 1993). In order to investigate regional differences in thermodynamic instability, we subsequently utilized NCEP Reanalysis data to construct regional mean tropospheric thermodynamic profiles (Fig. 8) of saturated equivalent potential temperature (θ_e*). These profiles were computed for a small subset of analysis domains including continental grid boxes over the Congo, AMZ, and N. Australia, and one isolated oceanic grid box in the western Pacific warm-pool.

Inspection of the lower tropospheric lapse rates of θ_e* (1000-700 mb; Fig. 8) combined with a consideration of the integrated instability (e.g., Convective Available Potential Energy; CAPE) observed in each profile (obtained by visually integrating parcel buoyancy utilizing values of temperature and specific humidity at p=1000 mb to compute a parcel θ_e), suggests that some consistency exists between regional mean CI and the TRMM-PR and LIS observations. For example, the Congo and N. Australia profiles exhibit more convective inhibition (CIN) and a much greater conditional instability ($\partial\theta_e$*/$\partial p > 0$) in the lowest 300 mb of the troposphere as compared to the AMZ and warm-pool profiles. Indeed, the AMZ θ_e* profile is similar to that observed over the warm-pool, both profiles exhibiting less CIN and less pronounced θ_e* lapse rates in the lower troposphere. Interestingly, visual inspection of the profiles suggests that the CAPE may not be all that different between the N. Australia, AMZ and warm-pool profiles. However, the "shape of the CAPE" favors more explosive, continental-like convection over N. Australia (Lucas et al., 1994) relative to the warm-pool and AMZ, consistent with the continental nature of the N. Australia RFDR. The Congo exhibits both larger CAPE and a more robust CI profile than any

15

of the other locations, again consistent with both the PR and LIS observations in the tropics. Though not shown in Fig. 8, studies such as Fu et al. (1999) suggest that the AMZ assumes a much more unstable θ_e^* profile during the transition season (Sept.-Nov.), also consistent with the TRMM PR (e.g., Fig. 7) and LIS data. Hence, to a first order it seems likely that a significant percentage of the variability in convective structure and associated lightning flash density between the various tropical locations can be explained by regional variability in the thermodynamic structure of the troposphere (e.g., Williams and Renno, 1993; Boccippio et al., 2000). Though not explored here, another likely candidate for explaining differences between regional mean convective structures includes the frequency and intensity of dynamical forcing associated with geographical location (e.g., coastal regimes in the sub-tropics; peninsular regions such as Florida etc.).

To summarize, note that many of the PR-sampled domains can be crudely classified as "tropical continental" or "tropical oceanic". However, with the exception of isolated oceanic regimes, the vertical precipitation structure observed within these classifications tends to exhibit a marked variability. Importantly, differences in regional mean deep convective structure may ultimately have implications for indicating the shape of mean diabatic heating profiles (e.g., Tao et al., 1990,1993), assessing errors in satellite-based precipitation estimates (McCollum et al., 2000) due to precipitation physics, and for computing upper atmospheric chemistry budgets (e.g., Jenkins, 2000) assuming that regional differences in the mean precipitation structure are a manifestation of differences in regional mean cloud kinematics.

4. Regional distributions of reflectivity as compared to ice-water content, lightning flash density and rainfall rate

In Sec. 3 it was suggested that differences in the RFDR's above the 5 km level may reflect an ever-increasing role for ice phase processes in the production of rainfall. This suggestion was based on the general observation that isolated oceanic RFDR's exhibit much smaller conditional probabilities of reflectivity ≥ 30 dBZ above the 5 km level, and much smaller Lightning Flash Densities (LFD's) as compared to the majority of their continental and coastal counterparts. As the host of previous studies

discussed in Sec. 1 suggest, lightning flash density should be a reliable proxy for overall trends in precipitation IWC. Therefore it is of interest to examine and quantify the relationship between precipitation IWC (estimated from Eq. 1) and LFD. Finally, if relationships between IWC, LFD, and rainfall rate are examined, evidence for the contribution by ice processes to both lightning and rainfall production should become apparent.

a.   Ice-water contents as a function of height

Several interesting features are revealed in the distributions of layer mean IWC when composited values for all analysis domains are plotted as a function of height (Fig. 9) for elevations above the 7 km level (~-12°C to -15°C). First, a continuum of IWC's is observed in Fig. 9 but an overall separation occurs between isolated oceanic domains possessing low IWC's and tropical and sub-tropical continental regimes possessing factor of two larger IWC's. Values of IWC intermediate to both the IO and continental regimes are found over the Amazon during the wet-season and over India during the monsoon. Variability in the IWC values for coastal regimes is also evident, especially the much larger values associated with convection situated over the Gulf Stream. Secondly (and as expected), the IWC profiles are highly correlated to the distributions of reflectivity values in excess of 30 dBZ (e.g., Fig. 7). Though reflectivities $\geq$ 30 dBZ typically comprise a small percentage ($\leq$ 20%) of the total sample at each height above 7 km (e.g., Fig. 7), the precipitation associated with these "deep convective mode" pixels at and above the 7 km level dominates the overall shape and amount of IWC observed. Over all, the general trend in wet-season IWC's bares a strong resemblance to the wet-season 85 GHz microwave brightness temperature cumulative distribution functions presented in Mohr et al. (1999).

b.   Ice-water contents and lightning flash density

TRMM-LIS LFD's and 7-9 km (~ -12°C to -30°C) layer mean IWC's plotted in Fig. 10 further elucidate regional/regime specific variations in precipitation microphysics and convective intensity. Not unexpectedly, IO regions are found consistently at low values of mixed phase region IWC and LFD,

while the reverse is generally true of continental regimes. The interior of the AMZ during its wet-season seems to best fit with oceanic or pronounced "monsoon" wet-season regimes such as that of India. Oceanic regions affected by nearby land masses (e.g., Gulf of Mexico, Gulf Stream, E. Pacific ITCZ near 10°S and 95°W; "ocean/coast" in Fig. 10) exhibit a broad range of characteristic IWC's and related LFD's that are also reflected in their respective reflectivity distributions (Figs. 5a-d).

The trend in LFD as a function of IWC in Fig. 10 suggests that a reasonably strong relationship exists between the precipitation IWC in the mixed phase region and LFD. If a least squares regression is applied to the LFD's as a function of the IWC, linear and quadratic fits yield R^2 values of 0.8 and 0.81 respectively. The fits do not greatly improve by increasing the degree of the polynomial fit. To some extent the linear to slightly non-linear trend in the relationship between IWC and LFD is to be expected. This can be illustrated by considering a simple precipitation based charging process that is based on a bulk microphysical continuous collection model. Assume:

1. the lightning flash rate (which will neutralize some amount of charge Q per unit time t) is proportional to the rate of charge generation in a cloud (dQ/dt).

2. an exponential size distribution [$N(D_p)=N_0 e^{-\lambda D_p}$] for precipitation ice species (graupel, hail, and snow); D_p = particle diameter; colliding in a continuous manner with smaller ice particles.

3. a monodisperse size distribution and negligible fallspeeds for smaller cloud ice particles of number concentration N_i.

4. charge transfers (δq) between precipitation ice and cloud ice depend on terminal fall speeds of precipitation ice particles (V_p) raised to the 2.5 power (e.g., $V_p^{2.5}$; Saunders et al., 1991).

Note that the flash-rate $\propto$ charging rate assumption in (3) will only be valid above some "threshold" in precipitation IWC and associated mixed phase conditions that permit significant charging to occur in the cloud (Takahashi, 1978; Saunders et al., 1991). Indeed, Fig. 10 would suggest that the threshold IWC, unique to this dataset, exists near a value of 0.12 g m^{-3}. Considering assumptions 1-4 above, the following relationships result:

$$\text{flash rate} \propto \frac{dQ}{dt} \propto \int_0^\infty N_i \Delta V_t V_p^{2.5} \delta q D_p^2 N_0 e^{-\lambda D} dD_p \tag{2}$$

$$\Delta V_t = V_p - V_{ice} \cong V_p = a V_p^b$$

$$\Downarrow$$

$$\therefore \text{flash rate} \propto \int_0^\infty D^{3.5b+2} e^{-\lambda D} dD = \frac{\Gamma(3.5b+3)}{\lambda^{3.5b+3}}$$

$$\lambda = \left(\frac{\pi \rho_p N_0}{\rho_{air} q_p} \right)^{0.25}$$

$$\text{with } q_p = IWC \quad \text{and} \quad b = 0.5$$

$$\therefore \text{flash rate} \propto N_i \, IWC^{1.2} \tag{3}$$

The resultant proportionality shown in (3) suggests that *the flash rate should be related to the precipitation IWC in an essentially linear fashion*, similar to the observed trend shown in Fig. 10. Equation (3) also underscores the need for smaller ice particles in the charge generation/separation process (Eq. 3 suggests that flash rate is proportional to the number concentration of small ice crystals; e.g., Baker et al., 1999). Buried in the constant of proportionality for (3) are variables such as the distribution intercept (N_0), particle density, and separation efficiency. Here we assume constant values for N_0 and ρ_i, and that separation efficiency is independent of D_p.

c. Precipitation production and lightning flash density

It was demonstrated in Sec. 4b that precipitation IWC's and LFD's are positively correlated for the regions studied (Fig. 10). If, in the mean, lightning flash density and precipitation IWC's are related to the mean convective vigor of a region, then it seems reasonable to infer that the presence of higher LFD's and precipitation IWC's (both indicative of more robust mixed phase microphysics) might also result in larger mean rainfall rates on a pixel by pixel basis. This also follows from studies such as DeMott and Rutledge (1998a) who found that maximum 30 dBZ heights (a measure of convective vigor) were better

correlated to instantaneous rainfall rate over the western Pacific warm-pool than cloud top heights (also used as a proxy for convective vigor). This relationship is explored in Figs. 11a-c by examining the mean instantaneous rainfall rate and LFD's as a function of the fraction of reflectivity pixels ≥ 30 dBZ located above the 7 km height level, and mixed phase region (7-9 km) precipitation IWC.

If depth of 30 dBZ reflectivity is a reflection of convective intensity (e.g., DeMott and Rutledge, 1998a), and if mixed phase ice processes contribute significantly to, or are a reflection of, heavy rainfall production, the rainfall rate and the regional fraction of 30 dBZ reflectivities found in cold regions of the clouds should be well correlated. Indeed, Fig. 11a suggests that this is the case. Upon converting the reflectivities to IWC's and focusing only on the middle of the mixed phase region of cloud between 7 km and 9 km (~-12° to -30° C), Fig. 11b reveals that a strong positive correlation exists between the mean rainfall rates and values of mixed phase IWC. To be consistent with Figs. 10 and 11a-b, we therefore expect regional mean rain rates to increase as a function of LFD, and indeed Fig. 11c suggests that this is the case. The same consistencies hold if the regional mean fraction of 30 dBZ pixels situated above the height of the 7 km level or regional mean 30 dBZ height are used instead of IWC (not shown).

Note that it is important to distinguish between the mean *instantaneous* rainfall rates measured by the TRMM, as presented in Figs. 11a-c, and a regional *total* rainfall amount. This is readily illustrated by again contrasting the Amazon and Congo. The mean 2-3 km instantaneous rainfall rate over the Congo (Amazon) measured by the TRMM-PR was 5.6 mm hr^{-1} (3.8 mm hr^{-1}). However, virtually all precipitation climatologies (Jaeger, 1976; Legates and Willmott, 1990; Xie and Arkin, 1997) and even the three year composite shown in Fig. 2a suggest that higher total rainfall amounts occur over the Amazon relative to the Congo during the December-March timeframe. To the extent that the precipitation climatologies are accurate, the combination of parameters presented in Figs. 10-11 suggests the presence of different rainfall regimes (e.g., Petersen and Rutledge, 1998; McCollum et al., 2000) in the Congo and Amazon basins. This view is further supported by studies such as Mohr and Zipser (1996; 1999) who noted that MCS's over tropical Africa exhibited the smallest median area but largest 85 GHz microwave brightness temperature depressions. Conversely, Mohr et al. (1999) noted that the intensity of Amazonian

MCS's was considerably weaker than that observed over the Congo, the former being more similar to that observed over the tropical oceans. More recently, after examining effective cloud droplet radii (e.g., Rosenfeld and Lentsky, 1998) and considering LIS LFD's over both the Amazon and central Africa (Christian et al., 1999), McCollum et al. (2000) hypothesized that precipitation production over the Congo was less maritime in nature (specifically involving more of a mixed phase ice phase process) than in other regions of the tropics including the Amazon. This finding is consistent with our inferences.

These results suggest that mixed phase ice processes likely play a larger role in, or at least accompany, the production of higher rainfall rates (as opposed to total rainfall) in regions of the tropics where copious amounts of lightning occur. This is due to the synergistic relationship between mixed phase microphysics, cloud kinematics and lightning. Though not examined here, one important question that remains unanswered concerns differences in the diabatic heating profile that might arise due to the regional variability in the precipitation process.

5.   Summary and conclusions

 We have examined the variability in vertical structure of precipitating clouds across a spectrum of geographical locations in the global tropics utilizing TRMM satellite radar reflectivity and lightning datasets. We constructed relative frequency distributions of TRMM-PR 2A-25 radar reflectivity as a function of height for approximately 22 oceanic and continental regions (grid boxes of 5-10° on each side) distributed throughout the global tropics. Ice water contents (derived from radar reflectivity) and TRMM 2A-25 algorithm mean rainfall rates for the 2-3 km layer were also computed for each grid box. Finally, to complement the radar analyses, TRMM-LIS lightning flash densities were also examined for the same regions.

Our analysis reveals that *isolated oceanic* rainfall exhibits remarkably little variability in precipitation structure across the tropics. All of the isolated oceanic grid boxes studied can be characterized as having deep clouds, heavy rainfall in the lowest 5 km of the troposphere and a factor of 10-100 decrease in lightning flash density relative to their continental counterparts. The relatively weak

vertical structure and reduced lightning flash densities (relative to tropical landmasses) were manifested in reflectivity histograms by an overall marked increase in the frequency of reflectivities ≥ (≤) 30 dBZ at levels below (above) the freezing level (~5 km). The implied predominance of warm-rain processes and dearth of lightning found over the tropical oceans was further supported by the presence of relatively low precipitation ice water contents in the mixed phase region of the clouds.

In contrast to "isolated" regions of ocean, *coastal* grid boxes or grid boxes located within ~1000 km of a continent, but over ocean, exhibited a much more variable behavior with regard to vertical structure. Reflectivity distributions combined with lightning and ice water contents from those regions suggest that the associated convection could be characterized as either similar to isolated oceanic (e.g., eastern equatorial Pacific), intermediate to isolated oceanic and continental (e.g., South China Sea, Gulf of Mexico), or continental (e.g., Gulf Stream) in its characteristics.

In general, as the rainfall regimes transitioned to become more "continental" in nature, the reflectivity structures at sub-freezing temperatures suggest an increased role for ice processes in the production of rainfall. In contrast to the isolated oceanic regimes however, the vertical structures of precipitation over the continents exhibited a marked spectrum of variability between the analyzed grid boxes, *especially at altitudes above the freezing level*. For example, grid boxes selected for this study that are located in the Amazon and India can all be considered "interior" to a tropical continent. However, composited reflectivity distributions, ice water contents and lighting flash densities observed during their respective *wet-seasons* exhibited characteristics similar to those observed over isolated regions of the tropical ocean with only a hint of the "continentality" observed over continental landmasses such as Northern Australia, the Congo, south-central Africa, and the southern U.S. With respect to the Amazon, this result is consistent with the *wet-season* passive microwave observations of MCS intensity (Mohr et al., 1999). However, seasonal variability is also pronounced in the Amazon, with vertical structures, precipitation ice water contents and lightning flash densities exhibiting robust "continental" characteristics during the *transition season* of September-November (this is also somewhat true over India when considering the monsoon and pre/post monsoon seasons; cf. Manohar et al., 1999).

Considering the spatial and even seasonal variability noted in the above observations it is clear that care must be used when applying simple geographical qualifiers such as "continental" or "oceanic" to describe convective morphologies.

The relative frequency of significant precipitation mass located above the freezing level *varied across a continuum*, beginning with isolated oceanic locations situated on the low end, transitioning to continental monsoon or rainforest regions such as India and the Amazon, and increasing to tropical and sub-tropical continental locations on the high end. Relative differences in this parameter have microphysical implications for both precipitation and electrification processes and may also reflect real differences in the diabatic heating profile. To further explore these differences regional-mean mixed-phase region ice water contents, lightning flash densities and rain rates in the 2-3 km height layer were correlated to look for consistencies between the parameters. The results are internally consistent, suggesting that a) precipitation ice water content and lightning flash density are highly correlated (this was also suggested via simple scaling considerations); b) precipitation ice water content and mean instantaneous rain rate are highly correlated; and c) lightning flash density and mean instantaneous rain rate are well correlated. The resultant correlations suggest that regions associated with higher lightning flash density will be associated with higher precipitation ice water contents and a more significant fraction of rainfall that is produced via mixed phase processes.

The observed relationships between precipitation ice water content and lightning flash density combined with scaling considerations suggest a potential application for global tropical measurements of ice water content and lightning flash density. To the extent that both flash density and ice water content can be accurately observed, and at least one of the variables can be accurately modeled, the results of this study suggest that either variable could be used as a component in a modeling inversion process that would retrieve the other variable. This might be useful in the future, for example, when studying the effect of climate change on the global electrical circuit or atmospheric chemical properties such as $N0_x$ production in a general circulation model. For example, if ice water content can be predicted in a GCM (e.g., Fowler et al., 1996), then it should also be possible to invert predicted ice water contents to retrieve

lightning flash density. Once flash densities were diagnosed, chemistry budget source terms dependent on lightning could also be retrieved. The inverse argument (e.g., flash density to ice water content) should also apply, though currently there are no GCM's that include lightning flash density as a prognostic variable.

Together, the TRMM-PR and LIS observations suggest the presence of a wide, but identifiable variety of vertical profiles of precipitation in the tropics. Further refinements in the categorization of these profiles (e.g., consideration of convective and stratiform components, sub-seasonal variability based on synoptic flow etc.) could be accomplished utilizing vertical structure information from the TRMM-PR combined with ancillary information provided by instruments such as the LIS. In turn, regional mean precipitation profiles described in this fashion can be readily used in a wide variety of applications ranging from validation of future modeling studies targeted at diagnosing regional diabatic heating profiles (e.g., Tao et al., 1990, 1993), studies of convective influences on the global electrical circuit and upper tropospheric water vapor (e.g., Price, 2000), to diagnosing errors in satellite based rainfall retrievals/climatologies due to differences in precipitation microphysics (e.g., McCollum et al., 2000).

6. References

Alexander, G. D., J. A. Weinman, V. M. Karyampudi, W. S. Olson, and A. C. L. Lee, 1999: The impact of the assimilation of rain rates from satellites and lightning on forecasts of the 1993 Superstorm. Mon. Wea. Rev., 127, 1433-1457.

Anyamba, E., E. Williams, J. Susskind, A. Fraser-Smith, M. Fullekrug, 2000: The manifestation of the Madden-Julian oscillation in global deep convection and in the Schuman resonance intensity. *J. Atmos. Sci.*, **57**, 1029-1044.

Baker, M. B., A. M. Blyth, H. J. Christian, J. Latham, K. L. Miller, A. M. Gadian, 1999: Relationships between lightning activity and various thundercloud parameters: Satellite and modeling studies. *Atmos. Res.*, **51**, 221-236.

Black, R. A., 1990: Radar reflectivity-ice water content relationships for use above the melting level in hurricanes. *J. Appl. Meteor.*, **29**, 955-961.

Boccippio, D. J., S. J. Goodman, and S. Heckman, 2000: Regional differences in tropical lightning distributions. *J. Appl. Meteor.*, in press.

Carey, L. D., and S. A. Rutledge, 2000: The relationship between precipitation and lightning in tropical island convection: A C-band polarimetric radar study. *Mon. Wea. Rev.*, 128, 2687-2710.

Cartwright, T. J., and P. S. Ray, 1999: Radar-derived estimates of latent heating in the subtropics. *Mon. Wea. Rev.*, **127**, 726-742.

Chang, D.-E., C. A. Moralles, J. A. Weinman, and W. S. Olson, 1999: Combined microwave and sferics measurements as a continuous proxy for latent heating in mesoscale model predictions. Proceedings, *11th International Conference on Atmospheric Electricity*, NASA, Guntersville, Alabama, June 7-11, 1999, pp 372-374.

Christian, H. J., R. J. Blakeslee, S. J. Goodman, D. A. Mach, M. F. Stewart, D. E. Buechler, W. J. Koshak, J. M. Hall, W. L. Boeck, K. T. Driscoll, and D. J. Boccippio, 1999: The Lightning Imaging

Sensor. *Proceedings, 11ᵗʰ International Conference on Atmospheric Electricity*, 7-11 June 1999, Huntsville, Alabama, pp. 746.

Cummins, K. L., M. J. Murphy, E. A. Bardo, W. L. Hiscox, R. B. Pyle, and A. E. Pifer, 1998: A combined TOA/MDF technology upgrade of the U.S. National Lightning Detection Network. *J. Geophys. Res*., **103**, 9035-9044.

DeMaria, M., 1985: Linear response of a stratified tropical atmosphere to convective forcing. *J. Atmos. Sci.*, 42, 1944-1959.

DeMott, C. A., and S. A. Rutledge, 1998a: The vertical structure of TOGA COARE convection. Part I: Radar echo distributions. *J. Atmos. Sci*., **55**, 2730-2747.

DeMott, C. A., and S. A. Rutledge, 1998b: The vertical structure of TOGA COARE convection. Part II: Modulating influences and implications for diabatic heating. *J. Atmos. Sci*., **55**, 2748-2762.

Dye, J. E., J. J. Jones, A. J. Weinheimer and W. P. Winn, 1989: Observations within two regions of charge during initial thunderstorm electrification. *Quart. J. R. Met. Soc*., **114**, 1271-1290.

Fowler, L. D, D. A. Randall, and S. A. Rutledge, 1996: Liquid and ice cloud microphysics in the CSU General Circulation Model. Part I: Model description and simulated microphysical processes . *J. Climate*, **9**, 489-529.

Fu, R., B. Zhu, and R. E. Dickinson, 1999: How do atmosphere and land surface influence seasonal changes of convection in the tropical Amazon? *J. Climate*, **12**, 1306-1321,

Fullekrug, M., and Frazer-Smith, A. C., 1997: Global lightning and climate variability inferred from ELF magnetic field variations. *Geophys. Res. Lett*., **24**, 2411-2414.

Goodman, S. J., and H. J. Christian, 1993: Global observations of lightning. Atlas of Satellite Observations Related to Global Change. Cambridge University Press, pp 191-219.

Goodman, S. J., D. E. Buechler, K. Knupp, K. Driscoll, and E. W. McCaul Jr., 2000: The 1997-1998 El Nino event and related wintertime lightning variations in the southeastern United States. *Geophys. Res. Lett*., **27**, 541-544.

Grecu, M., E. N. Anagnostou, and R. F. Adler, 2000: Assessment of the use of lightning information in satellite infrared rainfall estimation. J. Hydromet., 1, 211-221.

Hartman, D. L., H. H. Hendon, and R. A. Houze, Jr., 1984: Some implications of the mesoscale circulations in tropical cloud clusters for large scale dynamics and climate. *J. Atmos. Sci.,* **41***,* 113-121.

Hidayat, S., and M. Ishii, 1998: Spatial and temporal distribution of lightning activity around Java. *J. Geophys. Res*., **103**, 14001-14009.

Horel, J. D., and J. M. Wallace, 1981: Planetary scale atmospheric phenomena associated with the southern oscillation. *Mon. Wea. Rev*., **109**, 813-829.

Iguchi, T., and R. Meneghini, 1994: Intercomparison of single-frequency methods for retrieving a vertical rain profile from airborne or spaceborne radar data. *J. Atmos. Oceanic Tech*., **11**, 1507-1517.

Jaeger, L., 1976: Monatskarten des niederschiags fur die ganze erde. *Berichte des Deutscher Wetterdienste*, Offenbach, 33, pp and plates.

Jayaratne, E. R., 1993: Conditional instability and lightning incidence in Gabarone, Botswana. *Meteorol. Atmos. Phys.*, **52**, 159-175.

Jenkins, G. S., 2000: TRMM satellite estimates of convective processes in central Africa during September, October, November 1998: Implications for elevated Atlantic tropospheric ozone. *Geophys. Res. Lett*., **27**, 1711-1714.

Johnson, R. H., T. M. Rickenbach, S. A. Rutledge, P. E. Ciesielski and Wayne H. Schubert, 1999: Trimodal characteristics of tropical convection. *J. Climate*, 12, 2397-2418.

Jorgensen, D. P., and M. A. LeMone, 1989: Vertical velocity characteristics of oceanic convection. *J. Atmos. Sci.*, **46**, 621-640.

Kent, G. S., E. R . Williams, P.-H. Wang, M. P. McCormick, and K. M. Skeens, 1995: Surface temperature related variations in tropical cirrus cloud as measured by SAGE II. *J. Climate*, **8**, 2557-2594.

Kotaki, M., and C. Katoh, 1983: Global distribution of thunderstorm activity observed by the Ionosphere Sounding Satellite (ISS-b*). J. Atmos. Terr. Phys*., **45**, 833-847.

Kummerow, C., and L. Giglio, 1994a: A passive microwave technique for estimating rainfall and vertical structure information from space. Part I: Algorithm description. *J. Appl. Met*., **33,** 3-18.

Kummerow, C., and L. Giglio, 1994b: A passive microwave technique for estimating rainfall and vertical structure information from space. Part II: Applications to SSM/I data. *J. Appl. Met*., **33**, 19-34.

Kummerow, C., W. Barnes, T. Kozu, J. Shiue, and J. Simpson, 1998: *J. Atmos. Oceanic Tech*., **15**, 809-817.

Lau, K.-M, and L. Peng, 1987: Origin of low-frequency (intraseasonal) oscillations in the tropical atmosphere. Part I: Basic Theory. *J. Atmos. Sci*., **44**, 950-972.

Lee, A. C. L, 1986: An operational system for remote location of lightning flashes using a VLF arrival time difference technique. *J. Atmos. Oceanic Tech*., **3**, 630-642.

Legates, D. R., and C. J. Willmott, 1990: Mean seasonal and spatial variability in gauge corrected global precipitation. *Int. J. Climatol*., **10**, 111-127.

Lucas, C., E. J. Zipser, and M. A. LeMone, 1994: Convective available potential energy in the environment of oceanic and continental clouds: Corrections and comments*. J. Atmos. Sci*., 51, 3829-3830.

Manohar, G. K., S. S. Kandalgaonkar, and M. I. R. Tinmaker, 1999: Thunderstorm activity over India and the Indian southwest monsoon. *J. Geophys. Res*., **104**, 4169-4188.

Mapes, B. E., R. A. Houze Jr., 1993: Diabatic divergence profiles in western Pacific mesoscale convective systems. J. Atmos. Sci., 52, 1807-1828.

Mapes, B. E., 1993: Gregarious tropical convection. *J. Atmos. Sci*., **50**, 2026-2037.

McCollum, J. R., A. Gruber, M. B. Ba, 2000: Discrepancy between gauges and satellite estimates of rainfall in equatorial Africa. *J. Appl. Meteor*., **39**, 666-679.

Meneghini, R., T. Iguchi, T. Kozu, T. Kwanishi, H. Kuroiwa, K. Okamoto, and D. Atlas, 1999: The TRMM precipitation radar: Opportunities and challenges. Preprints, *29th International Conference*

on Radar Meteorology, American Meteorological Society, July 12-16, 1999, Montreal, Quebec, Canada, pp 621-624.

Mohr, K. I., and E. J. Zipser, 1996: Mesoscale convective systems defined by their 85-GHz ice scattering signature: Size and intensity comparison over tropical oceans and continents. *Mon. Wea. Rev*., **124**, 2417-2437.

Mohr, K. I., J. S. Famiglietti, and E. J. Zipser, 1999: The contribution to tropical rainfall with respect to convective system type, size and intensity estimated from 85-GHz ice-scattering signature. *J. Appl. Meteor*., **38**, 596-606.

Nesbitt, S. W., E. J. Zipser, and D. J. Cecil, 2000: A census of precipitation features in the tropics using TRMM: Radar, ice scattering and lightning observations. *J. Climate*, in press.

Olson, W. S., C. D. Kummerow, Y. Hong, W.-K. Tao, 1999: Atmospheric latent heating distributions in the tropics derived from satellite passive microwave radiometer measurements. *J. Appl. Meteor*., **38**, 633-664.

Orville, R. E., and R. W. Henderson, 1986: Global distribution of midnight lightning: September 1977 to August 1978. *Mon. Wea. Rev*., **114**, 2640-2653.

Petersen, W. A., S. A. Rutledge and R. E. Orville, 1996: Cloud-to-ground lightning observations from TOGA COARE: Selected results and lightning location algorithms. *Mon. Wea. Rev*., **124**, 602-620.

Petersen, W. A., 1997: Multi-scale process studies in the tropics: Results from lightning observations. Ph.D. Dissertation, Colorado State University, Department of Atmospheric Science, Paper No. 632, April 1997, pp 354.

Petersen, W. A., S. A. Rutledge, 1998: On the relationship between cloud-to-ground lightning and convective rainfall. *Journal of Geophysical Research*, 103, 14025-14040.

Petersen, W. A., R. C. Cifelli, S. A. Rutledge, B. S. Ferrier, and B. F. Smull, 1999: Shipborne dual-Doppler operations during TOGA COARE: Integrated observations of storm kinematics and electrification. *Bull. Amer. Meteorol. Soc*., 80, 81-97.

Puri, K., 1994: Modeling studies on the Australian summer monsoon. *Mon. Wea. Rev*., 2816-2837.

Reeve, N., and R. Tuomi, 1999: Lightning activity as an indicator of climate change. *Q. J. R. Meteorol. Soc*., **125**, 893-904.

Riehl, H. and J. S. Malkus, 1958: On the heat balance in the equatorial trough zone. *Geophysica*, **6**, 503-538.

Rosenfeld, D., and M. Lensky, Satellite-based insights into precipitation formation processes in continental and maritime convective clouds Institute of Earth Sciences. *Bull. Amer. Meteor. Soc*., **79**, 2457-2476.

Rutledge, S.A., E.R. Williams and T.D. Keenan, 1992: The Down Under Doppler and Electricity Experiment (DUNDEE): Overview and preliminary results. *Bull. Amer. Meteor. Soc.,* **73**, 3-16.

Rutledge, S. A., and W. A. Petersen, 1994: Vertical radar reflectivity structure and cloud-to-ground lightning in the stratiform region of MCSs: Further evidence for in situ charging in the stratiform region. *Mon. Wea. Rev*., **122**, 1760-1776.

Rutledge, S. A., W. A. Petersen, R. C. Cifelli and L. D. Carey, 2000: Early results from TRMM-LBA: Kinematic and microphysical characteristics of convection in distinct meteorological regimes. Preprints, *24th Conference on Hurricanes andTropical Meteorology*, American Meteorological Society, Ft. Lauderdale, Florida, May 29 – 2 June, 2000, pp 137-138.

Satori, G. and B. Zeiger, 1998: Anomalous behavior of Schumann resonances during the transition between 1995 and 1996. *J. Geophys. Res*., **103**, 14147-14155.

Satori, G. and B. Zeiger, 1999: El Nino related meridional oscillation of global lightning activity. *Geophys. Res. Lett*., **26**, 1365-1368.

Saunders, C. P. R., W. D. Keith, and R. P. Mitzeva, 1991: The effect of liquid water on thunderstorm charging. *J. Geophys. Res*., **96**, 11007-11017.

Simpson, J., R. F. Adler, and G.R. North, 1988: A proposed Tropical Rainfall Measuring Mission (TRMM) satellite. *Bull. Amer. Meteor. Soc.*, **69**, 278-295.

Steiner, M., R. A. Houze, Jr., and S. E. Yuter, 1995: Climatological characterization of three dimensional storm structure from operational radar and raingauge data. *J. Appl. Meteor*., **34**, 1978-2007.

Sui, C.-H., and K.-M. Lau, 1989: Origin of low-frequency (intraseasonal) oscillations in the tropical atmosphere. Part II: Structure and propagation of mobile wave-CISK modes and their modification by lower boundary forcings. *J. Atmos. Sci*., **46**, 37-56.

Szoke, E. J., E. J. Zipser, and M. A. LeMone, 1986: A radar study of convective cells in mesoscale systems in GATE. Part I: Vertical profile statistics and comparison with hurricanes. *J. Atmos. Sci*., **43**, 181-197.

Takahashi, T., 1978: Riming electrification as a charge generation mechanism in thunderstorms. *J. Atmos. Sci*., **35**, 1536-1548.

Takahashi, T., K. Suzuki, M. Orita, M. Tokuno, and R. de la Mar, 1995: Videosonde observations of precipitation processes in equatorial cloud clusters. *J. Meteor. Soc. Japan*, **73**, 509-534.

Tao, W.-K., J. Simpson, S. Lang, M. McCumber, R. Adler, and R. Penc, 1990: An algorithm to estimate the heating budget from vertical hydrometeor profiles. *J. Appl. Meteor*., **29**, 1232-1244.

Tao, W.-K., S. Lang, J. Simpson, and R. Adler, 1993: Further development and testing of the heating retrieval algorithm for TRMM. *J. Meteor. Soc. Japan*, **71**, 685-700.

Toracinta, R. E., and E. J. Zipser, 2000: Lightning and 85-GHz MCSs in the global tropics. *J. Appl. Meteor*., accepted for publication.

Trenberth, K. E., G. W. Branstator, and P. A. Arkin, 1988: Origins of the 1988 North American drought. Science, 242, 1640-1645.

Williams, E. R., 1992: Schumann resonance: A global tropical thermometer. *Science*, **256**, 1184-1187.

Williams, E. R., S. A. Rutledge, S. C. Geotis, N. Renno, E. Rasmussen, and T. Rickenbach, 1992: A radar and electrical study of tropical hot towers. *J. Atmos. Sci.,* **49**, 1386-1395.

Williams, E. R., and N. Renno, 1993: An analysis of the conditional instability of the tropical atmosphere. *Mon. Wea. Rev.,* **121**, 21-36.

Williams, E. R., 1994: Global circuit response to seasonal variations in global surface air temperatures. *Mon. Wea. Rev*., **122**, 1917-1929.

Xie P., and P. A. Arkin, 1997: Global precipitation: A 17-year monthly analysis based on gauge

    observations, satellite estimates, and numerical model outputs. *Bull. Amer. Meteor. Soc*., **11**, 2539-

    2558.

Yang, S., and E. A. Smith, 1999: Four-dimensional structure of monthly latent heating derived from

    SSM/I satellite measurements. *J. Climate*, **12**, 1016-1037.

Yuter, S. E., and R. A. Houze, Jr., 1995: Three dimensional kinematic and microphysical evolution of

    Florida cumulonimbus. Part II: Frequency distributions of vertical velocity, reflectivity, and

    differential reflectivity. *Mon. Wea. Rev*., **123**, 1941-1963.

Zipser, E. J., and K. R. Lutz, 1994: The vertical profile of radar reflectivity of convective cells: A strong

    indicator of storm intensity and lightning probability? *Mon. Wea. Rev.,* **122**, 1751-1759.

Zipser, E. J., 1994: Deep cumulonimbus cloud systems in the tropics with and without lightning. *Mon.*

    Wea. Rev., **122**, 1837-1851.

Figure Captions

Figure 1. TRMM-LIS lightning flash densities for a) December-February 1998-2000; and b) June-August

1998-1999. TRMM-PR analysis boxes are also indicated (22 locations).

Figure 2. NCEP Reanalysis data composite means for austral summer (December-February 1998-2000):

a) precipitation (mm day^{-1}); and b) Outgoing Longwave Radiation (W m^{-2}).

Figure 3. As in Fig. 1 except September-November 1998-1999.

Figure 4. Wet-season relative frequency distributions of radar reflectivity (RFDR's) for isolated oceanic

locations (Table 1). Reflectivity is binned every 5 dBZ and plotted on the Y-axis, 1 km height bins are

plotted on the X-axis, and relative frequencies are plotted on the Z-axis. Wet-season months utilized in

the analysis are indicated at the top of each plot. a) western Pacific warm pool; b) eastern Equatorial

Atlantic ITCZ; c) Indian Ocean; d) west-central Pacific Ocean.

Figure 5. As in Fig. 4 but for coastal oceanic locations. a) Gulf Stream; b) South China Sea; c) Gulf of

Mexico; d) eastern equatorial Pacific Ocean.

Figure 6. As in Fig. 4 but for tropical continental locations. a) Congo; b) northern Australia; c) central

Amazon; d) southern India.

Figure 7. As in Fig. 4, but relative frequency of reflectivities in excess of 30 dBZ for a representative

subset of the grid boxes analyzed (Table 1). Locations are indicated on the X-axis. The approximate

wet/warm-season height of the -10°C isotherm is indicated in white. The relative frequencies for each

location are color shaded by regime.

Figure 8. Vertical profiles of θ_e* (K; solid lines) plotted as a function of pressure (ordinate) for the

Congo, Amazon (AMZ), northern Austalia, and the western Pacific warm-pool (W. Pool). Values of θ_e

are plotted (dashed lines) for values of temperature and specific humidity corresponding to the 1000 mb

level.

Figure 9. Seasonal mean precipitation ice water contents (g m^3; ordinate) plotted as a function of height (km; abscissa) and composited for the subset of regimes indicated on the bottom of the figure (see text). Regime types are indicated by the line on the inside left of the plot, ranging from continental to oceanic.

Figure 10. Wet-season mean LIS lightning flash densities (Flashes/km^2/month; ordinate) plotted vs. 7-9 km layer mean ice water contents (IWC; g m^{-3}, abscissa). Note that different markers (upper left corner) are utilized to indicate different regime types. Individual locations are indicated including values for the Amazon-transition season.

Figure 11. Scatter plots of wet-season mean a) rainfall rate (mm hr^{-1}; ordinate) vs. number (fraction) of reflectivity pixels above 7 km greater than 30 dBZ normalized by the number of raining pixels in the 2-3 km layer (abscissa); b) as in (a), but rainfall rate plotted vs. the 7-9 km layer mean ice water content (g m^{-3}; abscissa); c) as in (a), but rainfall rate plotted vs. LIS lightning flash density (flashes/km^2/month; abscissa). Linear regression and R^2 values are indicated in each plot.

Table 1: Analysis domains

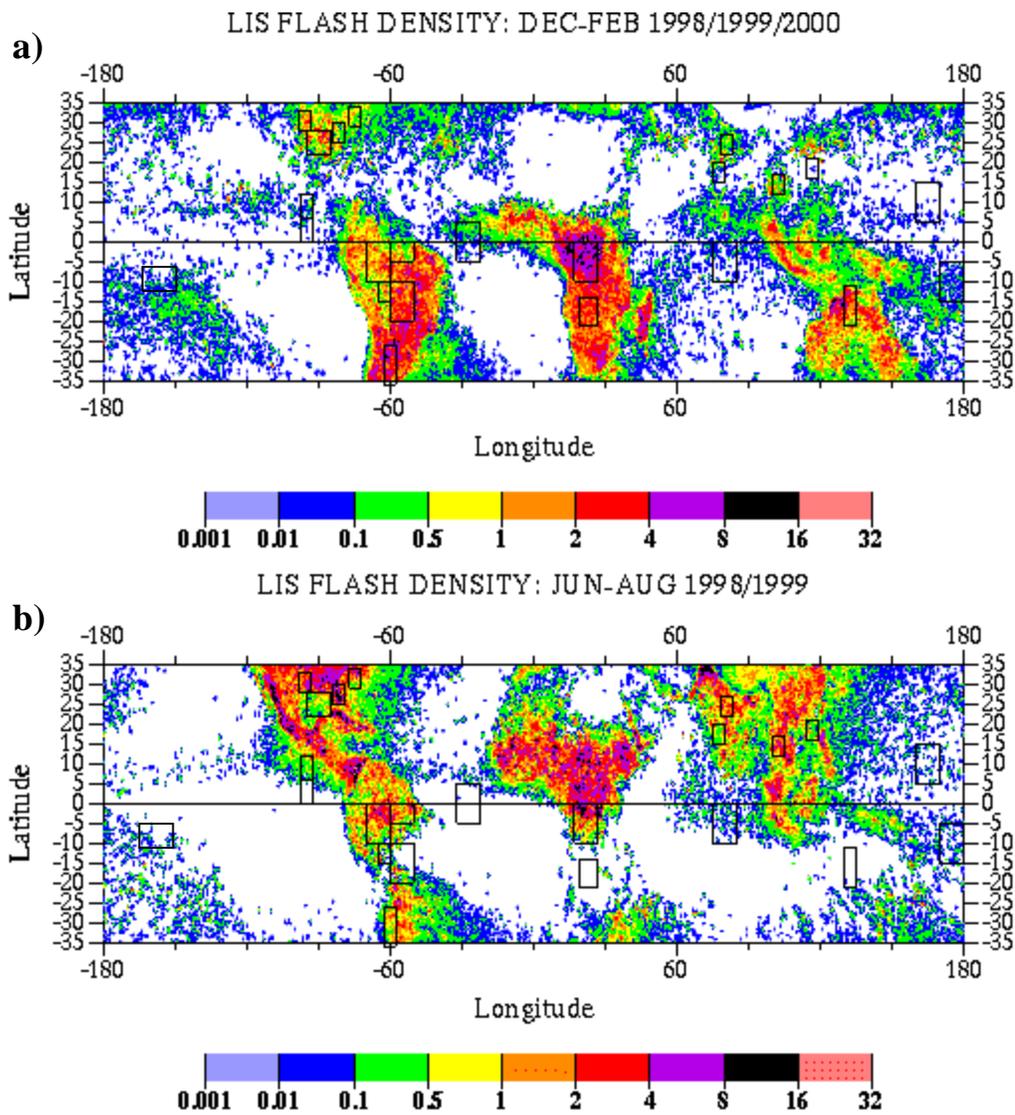| Location and Selected wet-season months ( )	Area Boundaries (Lat/Lon°)	Geographical Identifier
Congo, Africa (DJF)	0°S - 10°S / 17°E - 27°E	Tropical Continental
Sub-Congo, Africa (DJF)	14°S - 21°S / 19°E - 21°E	Tropical Continental
N. Australia, Australia (DJF)	11°S - 21°S / 130°E - 135°E	Tropical Continental
C. Amazon (AMZ) S. America (DJF)	0°S - 10°S / 60°W - 70°W	Tropical Continental
SW Amazon, S. America (DJF)	10°S - 15°S / 60°W - 65°W	Tropical Continental
E. Amazon, S. America (DJF)	0°S - 5°S / 50°W - 60°W	Tropical Continental
Mato Grosso, S. America (DJF)	10°S - 20°S / 50°W - 60°W	Tropical Continental
Thailand/Cambodia, SE Asia (JJA)	12°N - 17°N / 100°E - 105°E	Tropical Continental
S. India, India (JJA)	15°N - 20°N / 75°E - 80°E	Tropical Continental (monsoon)
W. Pacific warm-pool (DJF)	5°S - 15°S / 170°E - 180°E	Tropical Isolated Oceanic
W. Central Pacific (JJA)	5°N - 15°N / 160°E - 170°E	Tropical Isolated Oceanic
E. Equatorial Atlantic (DJF)	5°N - 5°S / 22°W - 32°W	Tropical Isolated Oceanic
Indian Ocean (DJF)	0°S - 10°S / 75°E - 85°E	Tropical Isolated Oceanic
C. Eq. Pacific (DJF)	6°S - 11°S / 155°W - 165°W	Tropical Isolated Oceanic
Argentina, S. America (DJF)	26°S - 36°S / 57°W - 63°W	Subtropical Continental
N. India, India (JJA)	22°N - 27°N / 78°E - 83°E	Subtropical Continental (monsoon)
Florida, N. America (JJA)	25°N - 30°N / 79°W - 84°W	Subtropical Continental
SE U.S., N. America (JJA)	28°N - 35°N / 93°W - 100°W	Subtropical Continental
E. Eq. Pacific (JJA)	6°N - 12°N / 92°W - 97°W	Tropical coastal/oceanic
S. China Sea (JJA)	16°N - 21°N / 114°E - 119°E	Tropical coastal/oceanic
Gulf Stream, (JJA)	29°N - 34°N / 72°W - 77°W	Subtropical coastal/oceanic
Gulf of Mexico, (JJA)	22°N - 28°N / 85°W - 95°W	Subtropical coastal/oceanic

Figure 1. TRMM-LIS lightning flash densities for a) December-February 1998-2000; and b) June-August
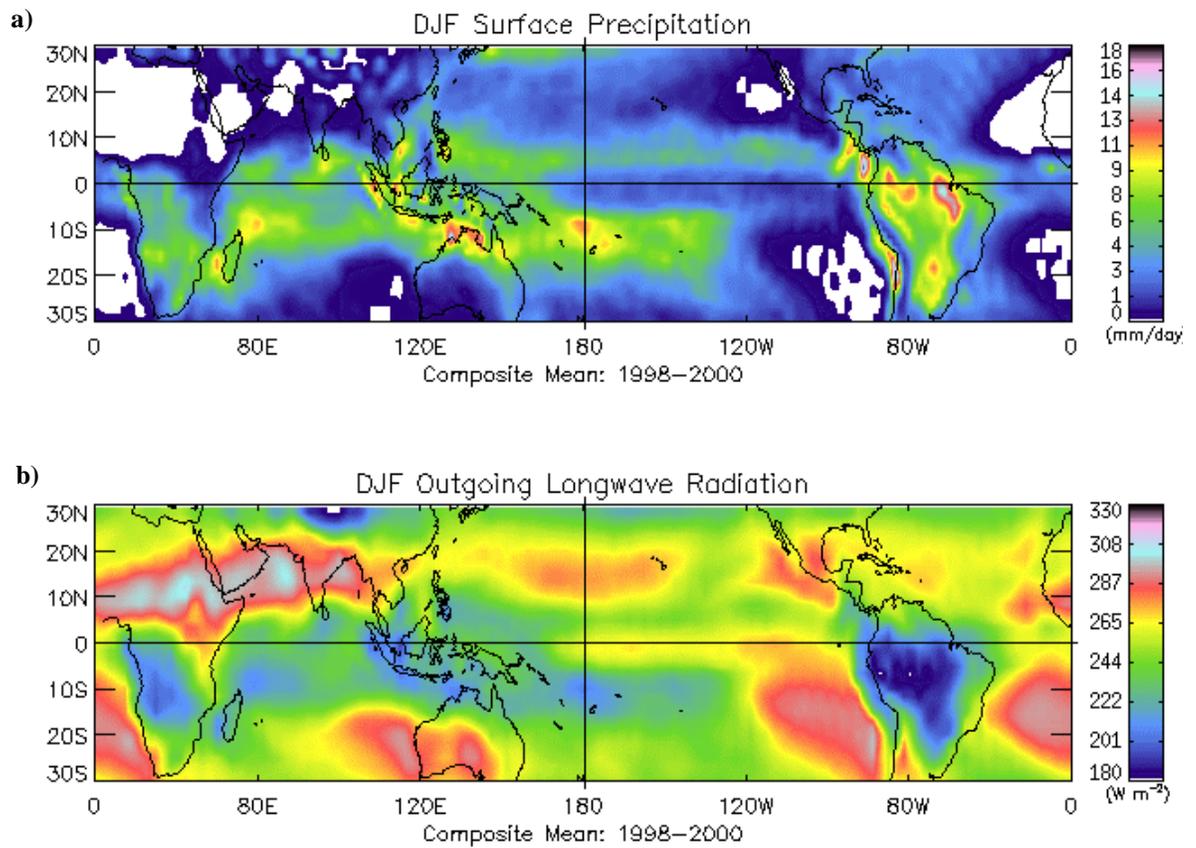1998-1999. TRMM-PR analysis boxes are also indicated (22 locations).

Figure 2. NCEP Reanalysis data composite means for austral summer (December-February 1998-2000):

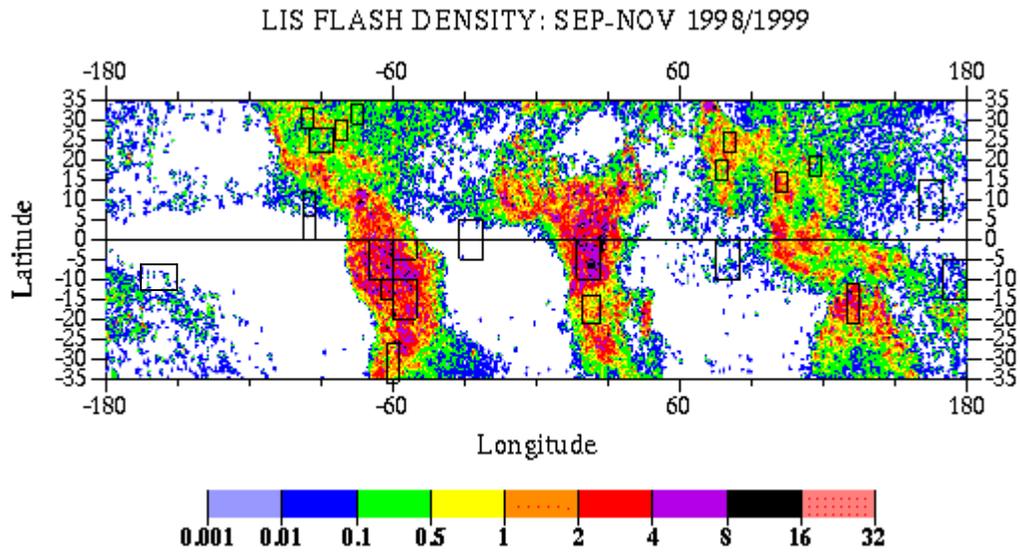a) precipitation (mm day^{-1}); and b) Outgoing Longwave Radiation (W m^{-2}).

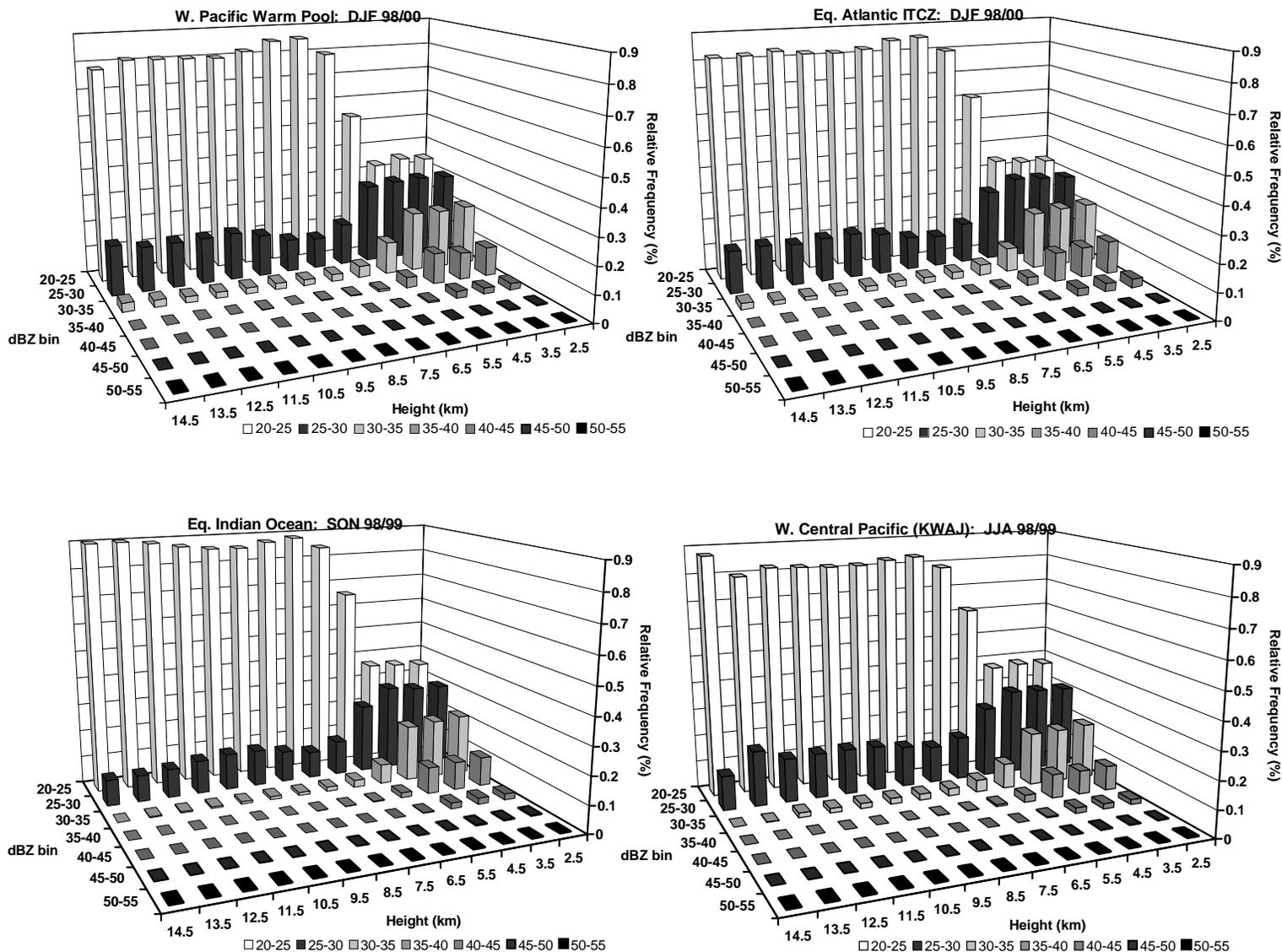Figure 3. As in Fig. 1 except September-November 1998-1999.

Figure 4. Wet-season <u>r</u>elative <u>f</u>requency <u>d</u>istributions of radar <u>r</u>eflectivity (RFDR's) for isolated oceanic locations (Table 1). Reflectivity is binned every 5 dBZ and plotted on the Y-axis, 1 km height bins are plotted on the X-axis, and relative frequencies are plotted on the Z-axis. Wet-season months utilized in the analysis are indicated at the top of each plot. a) western Pacific warm pool; b) eastern Equatorial Atlantic ITCZ; c) Indian Ocean; d) west-central Pacific Ocean.

Figure 5. As in Fig. 4 but for coastal oceanic locations. a) Gulf Stream; b) South China Sea; c) Gulf of

Mexico; d) eastern equatorial Pacific Ocean.

Figure 6. As in Fig. 4 but for tropical continental locations. a) Congo; b) northern Australia; c) central

Amazon; d) southern India.

Figure 7. As in Fig. 4, but relative frequency of reflectivities in excess of 30 dBZ for a representative subset of the grid boxes analyzed (Table 1). Locations are indicated along the Y-axis. The approximate wet/warm-season height of the -10°C isotherm is indicated in white. The relative frequencies for each location are color shaded by regime.
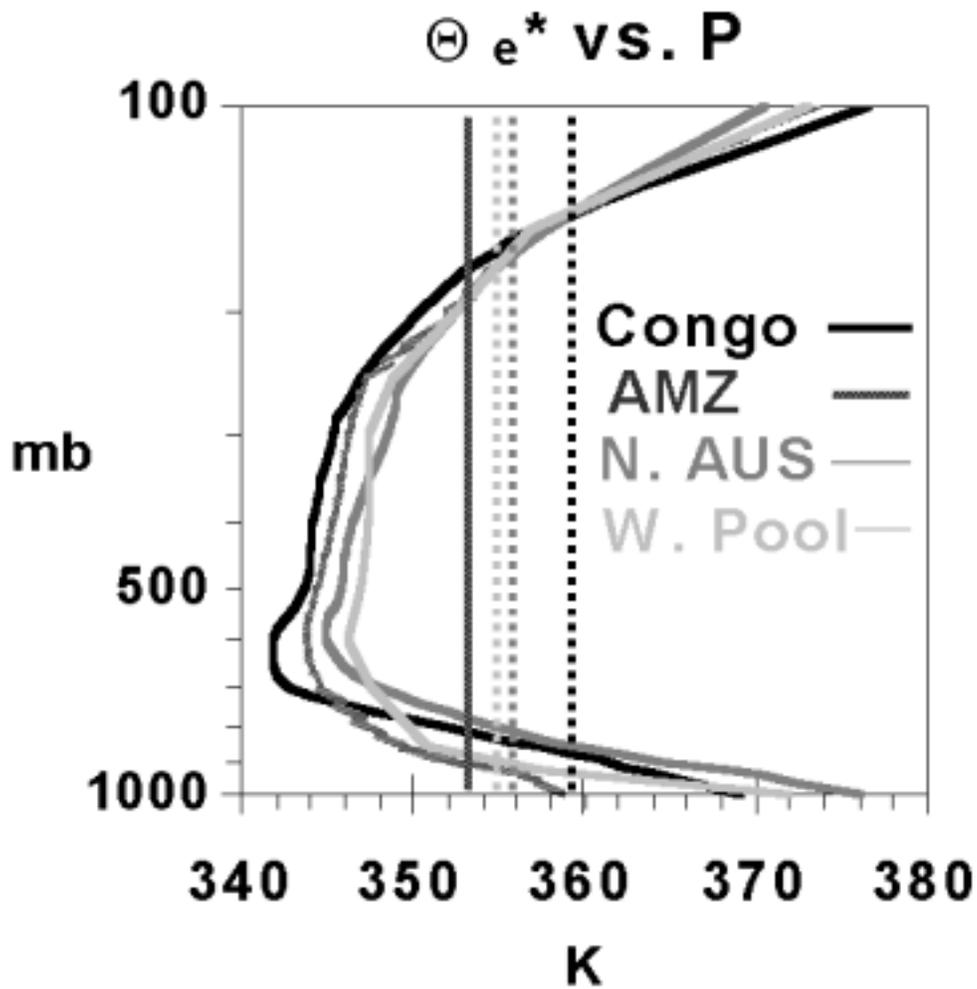
Figure 8. Vertical profiles of θ_e* (K; colored solid lines) plotted as a function of pressure (ordinate) for the Congo, Amazon (AMZ), northern Austalia, and the western Pacific warm-pool (W. Pool). Values of θ_e are plotted (colored dashed lines) for values of temperature and specific humidity corresponding to the 1000 mb level.

TRMM PR: WARM/WET SEASON 1998-2000
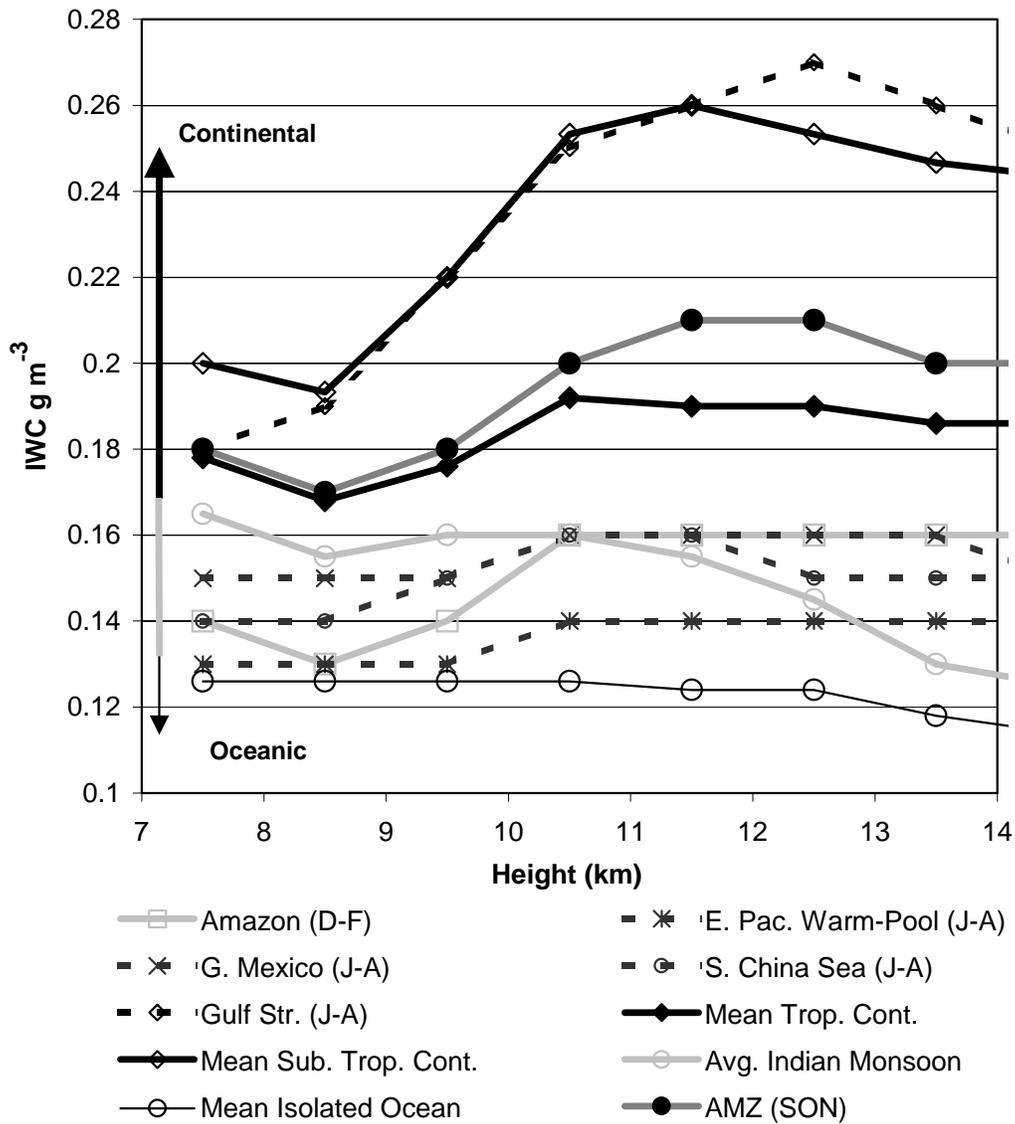**Conditional Mean Ice Water Content (g m^3)**

Figure 9. Seasonal mean precipitation ice water contents (g m^3; ordinate) plotted as a function of height (km; abscissa) and composited for the subset of regimes indicated on the bottom of the figure (see text). Regime types are indicated by the line on the inside left of the plot, ranging from continental to oceanic.

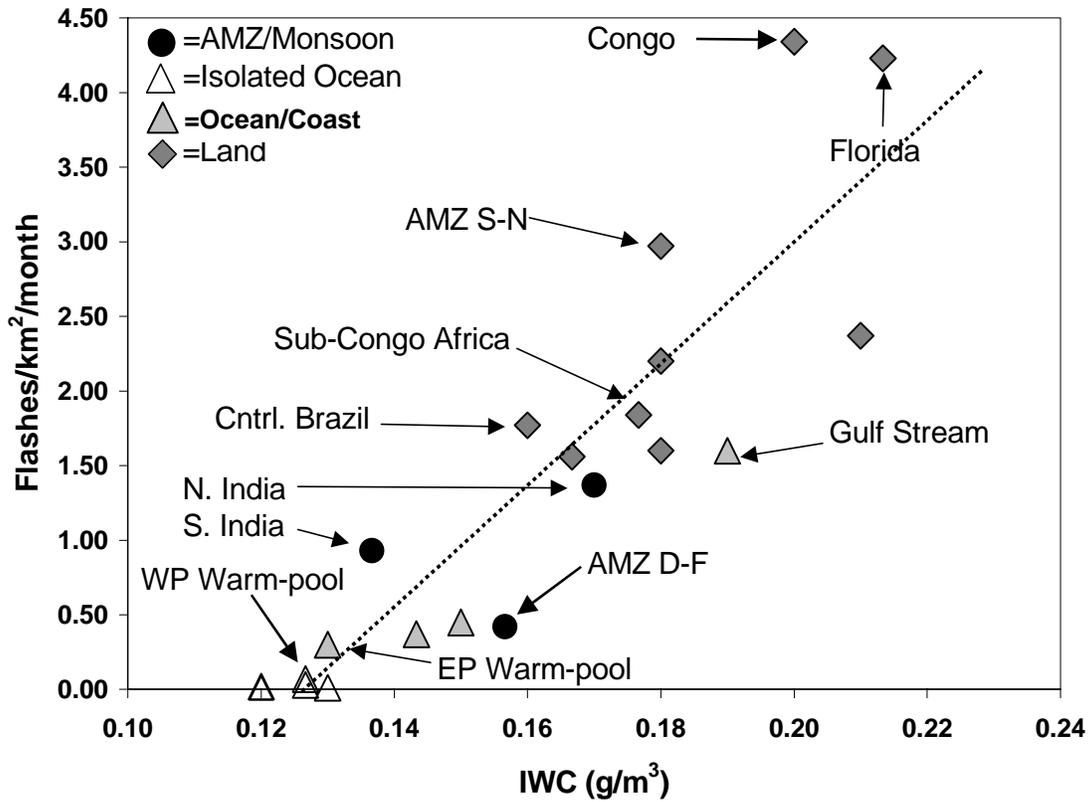**Wet Season (1998-2000): LIS Flash Density vs. IWC (7-9 km)**

Figure 10. Wet-season mean LIS lightning flash densities (Flashes/km^2/month; ordinate) plotted vs. 7-9 km layer mean ice water contents (IWC; g m^{-3}, abscissa). Note that different markers (upper left corner) are utilized to indicate different regime types. Individual locations are indicated including values for the Amazon-transition season.
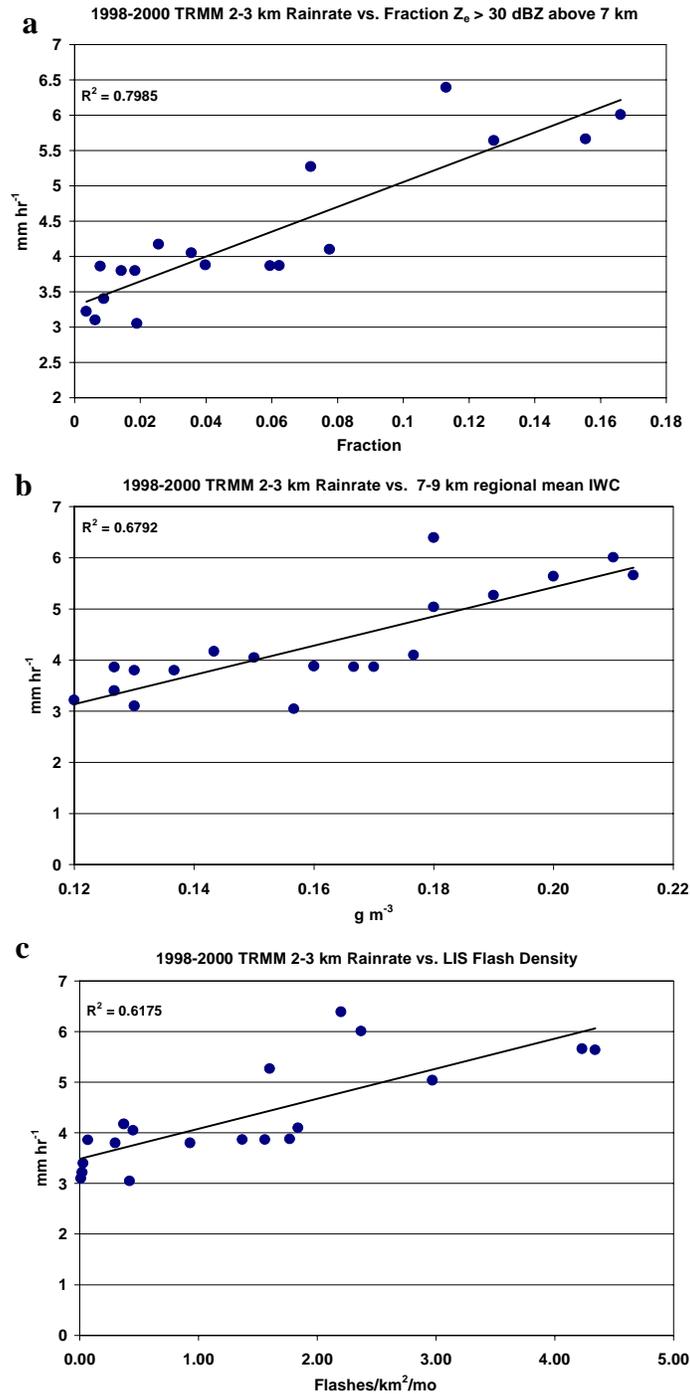
Figure 11. Scatter plots of wet-season mean a) rainfall rate (mm hr-1; ordinate) vs. number (fraction) of reflectivity pixels above 7 km greater than 30 dBZ normalized by the number of raining pixels in the 2-3 km layer (abscissa); b) as in (a), but rainfall rate plotted vs. the 7 - 9 km layer mean ice water content (g m^{-3}; abscissa); c) as in (a), but rainfall rate plotted vs. LIS lightning flash density (Flashes/km^2/month; abscissa). Linear regression and R^2 values are indicated in each plot.